Non-muffin-tin and relativistic interaction effects on the electronic structure of noble metals

A. H. MacDonald

National Research Council, Ottawa, Canada K1A 0R6

J. M. Daams* and S. H. Vosko

University of Toronto, Toronto, Canada M5S 1A7

D. D. Koelling

Argonne National Laboratory, Argonne, Illinois 60439

We report self-consistent-field calculations for the noble metals Cu, Ag, and Au. This work represents an improvement on previous work in that we have included (self-consistently) both non-muffin-tin terms in crystal potential and relativistic effects in the kinematics (by solving the single-particle Dirac equation) and in the interactions (by employing a relativistic correction to the exchange-correlation potential). The significance of these improvements has been examined by a comparison of different versions of our own calculations with previous calculations, and by a comparison with experiments. An important result obtained is that the Fermi-surface discrepancy previously reported for Cu is greatly reduced without the necessity of artificially increasing the strength of the exchange-correlation potential.

I. INTRODUCTION

This paper describes the results of self-consistent relativistic band-structure calculations for the noble metals Cu, Ag, and Au which we performed using relativistic kinematics and no muffin-tin or other type of "shape" approximation. Non-muffin-tin, relativistic, and self-consistency effects have, to our knowledge, not been previously included together for any of the noble metals. The exchange-correlation (xc) potentials used in this work are those implied by the local density approximation (LDA) of the density functional formalism[1] and we interpret our results in terms of that formalism. Thus we will first consider the ground-state properties which would be given exactly by the density functional formalism if the exact functional were used rather than the LDA. We, however, also examine the Fermi surface and quasiparticle properties on that surface, which entails further approximation.[2] Work, primarily in the alkali metals, has indicated that this level of approximation is not adequate.[3-7] It will be seen, however, that this approximation is much better than previously thought for the noble metals.

In the relativistic version of the density functional formalism[9,10] a relativistic correction to the

xc potential appears naturally. This correction, which primarily represents the influence of the current-current interaction, has been used in few band-structure calculations to date even when relativistic kinematics are included. As part of a continuing study of its significance, we examine its effects for the noble metals. We present detailed results for the influence of the relativistic exchange (rx) correction on the self-consistent charge densities and crystal potentials and on core and valence level eigenvalues. The xc potentials we have used may be written as

$$\mu_{xc}(r_s) = \frac{-2}{\pi \alpha r_s} \left[\psi^{rx}(r_s) + \frac{1}{2} \pi \alpha C r_s \ln \left[1 + \frac{A}{r_s} \right] \right] \tag{1a}$$

in units of Ry where the parameters A and C characterize the correlation contribution to the potential[11] and the rx correction factor, which is identically 1 in the nonrelativistic exchange case nx, is given by[10,12]

$$\psi^{rx}(r_s) = -\frac{1}{2} + \frac{3 \ln[\beta + (1+\beta^2)^{1/2}]}{2\beta(1+\beta^2)^{1/2}} , \tag{1b}$$

where $r_s = (3/4\, \pi n a_0^3)^{1/3}$ is the usual conduction electron density parameter and $\beta = 1/171.4 r_s$. We will refer to the calculations for which $\psi^{rx}(r_s)$ has been set equal to one as the nx calculations, and to the calculations which used Eq. (1b) for ψ^{rx} as the rx calculations. We have also performed self-consistent calculations with the correlation contribution to the xc potential set to zero and we refer to these as the xo (exchange-only) calculations. The computational methods used in this calculation have been described elsewhere in some detail.[13-15]

In Sec. II we discuss our results for the self-consistent crystal potentials and charge densities. The single-particle eigenvalues obtained are presented and compared with appropriate experiment in Sec. III while in Sec. IV we discuss the Fermi surfaces obtained in this calculation. Finally in Sec. V, we discuss the Pauli susceptibility of the noble metals. Section VI contains some concluding remarks.

II. CHARGE DENSITIES AND CRYSTAL POTENTIALS

The non-muffin-tin contribution to the self-consistent charge density inside the muffin-tin spheres is illustrated in Figs. 1 and 2 by plotting the $L = 4$ and 6 components of its Kubic harmonic expansion:

$$4\pi r^2 \rho(\vec{r}) = \sigma_0(r) + \sigma_4(r) K_4(\hat{r})$$

$$+ \sigma_6(r) K_6(\hat{r}) , \qquad (2a)$$

$$K_4(\hat{r}) = \frac{\sqrt{21}}{4r^4}[5(x^4 + y^4 + z^4) - 3r^4] , \qquad (2b)$$

$$K_6(\hat{r}) = \frac{\sqrt{13/2}}{8r^6}[462x^2y^2z^2$$

$$+ 21r^2(x^4 + y^4 + z^4) - 17r^6] . \qquad (2c)$$
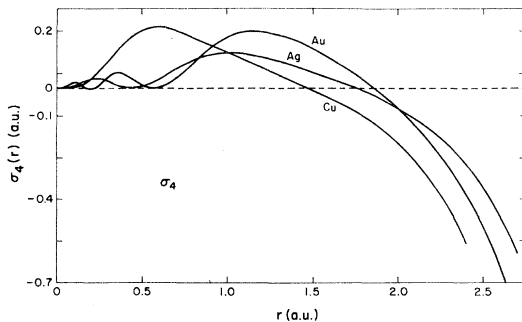
From the curves for $\sigma_4(r)$ it is clear that except near the muffin-tin-sphere boundary most of the contribution to this quantity comes from the $3d$, $4d$, and $5d$ wave functions for Cu, Ag, and Au, respectively. The radial dependence of $\sigma_6(r)$ suggests that it results primarily from the reexpansion, about one atomic site, of localized wave functions centered on neighboring atomic sites. The smaller magnitude $\sigma_6(r)$ for Ag compared to Cu and Au is due to Ag having more localized d-wave functions. We note that the non-muffin-tin terms in the charge density for the noble metals are very similar at the muffin-tin-sphere boundary to those obtained[13] for Pd and Pt but that the d-wave-like peaks in $\sigma_4(r)$ in the interior region are smaller in the noble-metal case. This again reflects the fact that near the sphere boundary non-muffin-tin terms come from the inhomogeneity of the crystal while the asphericity of the charge-density around each atomic site dominates at smaller values of r. This asphericity is smaller for the noble metals than for Pd and Pt because the d band of the noble metal is more nearly filled.

As the fundamental variable in density functional theory, the charge density is certainly one feature that should be yielded correctly by the computation. X-ray scattering factors give direct evidence as to the nature of the charge density so it is desirable to compare the calculated results to that experimental data. Unfortunately, the experiment becomes more difficult with increasing atomic number so that copper is near the present limit of practicality, and we can perform such a comparison only for Cu. Both the experimental and the theoretical situations have been summarized recently by Schneider et al.[16] and we make extensive use of their tabulations. The experimental situation is still characterized by considerable scatter. This is due to both the difficulty of making corrections for extinction, multiple scattering, and ther-

FIG. 1. Self-consistent $\sigma_4(r)$ for Cu, Ag, and Au.
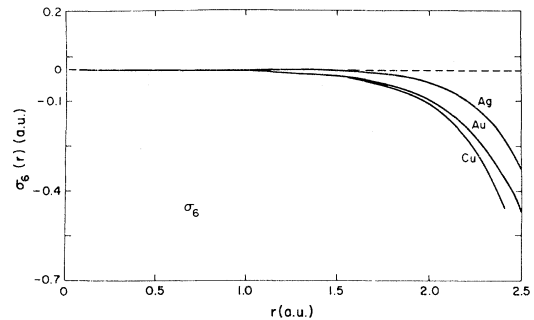
FIG. 2. Self-consistent $\sigma_6(r)$ for Cu, Ag, and Au.

mal motion in the data and to the difficulty in acquiring sufficiently precise data. With these provisos, we may still compare our results to the experimental data and draw a few tentative conclusions. We choose to select the (111), (200), (222), and (333)/(511) reflections for examination. This is because there seems to be the best agreement among experiments for these reflections and the (333)/(511) pair provide the first pair to reveal anisotropy. In Table I, we display the single-crystal results of Jennings et al.[17] and Freund[18] and the γ-ray results of Schneider et al.[16] on mosaic crystals. Note that the results of Jennings et al. on single crystals agree reasonably well with results of Schneider et al. and that the results of Schneider et al. probably err toward smaller values. The theoretical calculations of Snow[19] and of Arlinghaus[20] are included as well as the present work. First consider the anisotropy represented by the (333)/(511) reflections. Only Schneider et al. report any difference in these two reflections and they are inside the error bars. This is quite consistent with the essentially filled d shell of Cu. However, if one believes that there is a small difference indicated, then it is larger than in the calculations. This would be quite consistent with the situation found in vanadium[21] where a $t_{2g} - \epsilon_g$ split is required together with some orbital adjustments.

The calculated form factors appear to be slightly too large implying a charge density somewhat too tightly bound to the atom. Our xo calculation differs from that of Snow[19] for $\alpha = \frac{2}{3}$ in that we have included relativistic kinematics and non-muffin-tin effects, and sampled the Brillouin zone more carefully. The resulting differences are quite

small [0.06 for (111), 0.04 for (200), 0.07 for (222)], indicating a relative insensitivity of the charge density to these improvements. Our results are all larger than Snow's indicating that the net effect of the relativistic corrections was a small contraction of the charge density. The inclusion of the correlation potential has a similar and only slightly larger effect. For Cu, we have performed calculations both for a low temperature ($a = 6.809$) and room temperature ($a = 6.8309$) lattice constant; the size of the change in form factor with lattice constant is also of similar magnitude. The smaller lattice constant yielded smaller form factors consistent with greater itinerancy of the electrons. These changes are an appreciable fraction of the difference between the calculated and measured form factors. Nonetheless, a discrepancy does appear to remain. The calculation of Arlinghaus[20] using the Chodorow potential and Hartree-Fock atomic core densities still appears to give the best agreement with experiment. This is interesting in that the Chodorow potential is a model potential constructed to yield the same $3d$ orbitals as the full Hartree-Fock (no local density approximation) atomic calculation. Thus this phenomenological local potential might be including exchange effects more reliably than the standard local density approximation.

The influence of the rx correction on the self-consistent charge densities is illustrated in Fig. 3. For Au, the influence of local correlation on the self-consistent charge density is also shown by plotting the difference between the results of xo and nx calculations. The local correlation potential, which is attractive and larger in magnitude at higher density, shifts charge toward the nucleus.

TABLE I. Comparison of experimental and theoretical scattering form factors for Cu.

($hk1$)	Jennings et al.[a] (1964)	Freund[b]	Schneider et al.[c] (1981)	xo ($a = 6.809$)	nx ($a = 6.831$)	Snow[d] ($\alpha = 1$) ($a = 6.831$)	Snow[d] ($\alpha = \frac{2}{3}$) ($a = 6.831$)	Arlinghaus[e] (Chodorow)
(111)	21.52(10)	22.63	21.38(9)	21.65	21.73	22.33	21.63	21.54
(200)			20.10(6)	20.32	20.39	21.04	20.40	20.25
(222)	14.01(10)	14.64(10)	13.99(8)	14.19	14.25	14.53	14.16	13.90
(333)	9.41(10)	9.54(10)	9.45(9)	9.63	9.66			9.51
(511)			9.49(6)	9.64	9.67			

[a]Reference 17.
[b]Reference 18.
[c]Reference 16.
[d]Reference 19.
[e]Reference 20.
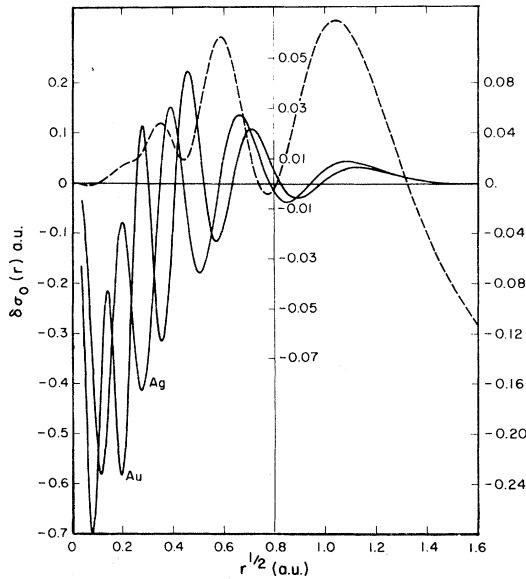
FIG. 3. Changes in the self-consistent $\sigma_0(r)$ for Ag
and Au due to changes in the xc potential. The solid
curves give the changes produced by the relativistic ex-
change correction with the left axis giving the scale for
Au and the right axis the scale for Ag. The dashed
curve shows the change produced by the correlation con-
tribution to the local potential. The vertical scale in the
middle of the figure corresponds to this curve.

On the other hand, the rx correction, which is
repulsive and increases sharply in magnitude as
density increases in the deep core region, generally
shifts charge away from the nucleus. The minima
and maxima of the rx density correction curve gen-
erally reflect peaks in the density contributions
from individual orbitals in the nx and rx potential,
respectively. We note that, as expected, the rx den-
sity corrections are reduced in the lighter atoms;
the corrections decrease by a factor of about 3 in
going from Au to Ag and by a further factor of 3
in going from Ag to Cu (not shown).

The non-muffin-tin components of the self-
consistent crystal potentials are presented in Fig. 4.
The non-muffin-tin terms are roughly the same for
Ag and Au and roughly the same in form but
smaller than those obtained[13] for Pd and Pt. They
are slightly larger for Cu and more comparable to
the Pd and Pt results. These non-muffin-tin con-
tributions to the potential are dominated by elec-
trostatic contributions, especially near the muffin-
tin-sphere boundary. Relative to relevant energy
scales, such as the d-band widths or free-electron
Fermi energies, the magnitude of the non-muffin-
tin terms cannot be regarded as small. Neverthe-
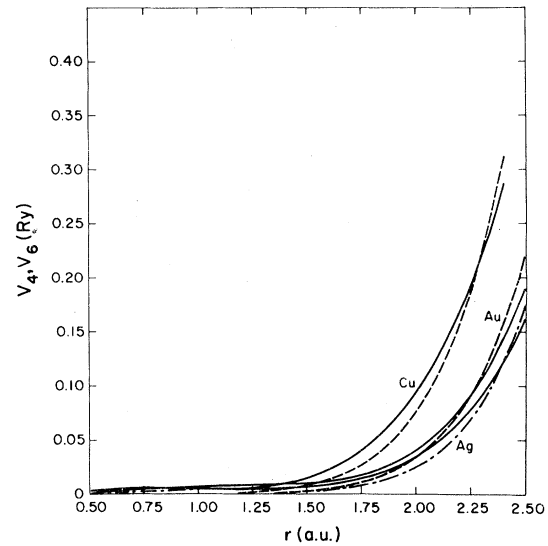
FIG. 4. Kubic Harmonic expansion coefficients $V_4(r)$
and $V_6(r)$ for the non-muffin-tin terms in the self-
consistent crystal potentials of Cu, Ag, and Au. The
solid curves give $V_4(r)$ and the dashed curves give $V_6(r)$.

less, the changes in single-particle energies pro-
duced by these terms are fairly small ($\lesssim 10$
mRy).[22]

The influence of the rx correction on the crystal
potential is shown in Fig. 5 along with, for the
case of Au, the local correlation influence. The rx
correction makes a repulsive contribution to the
crystal potential which increases sharply in magni-
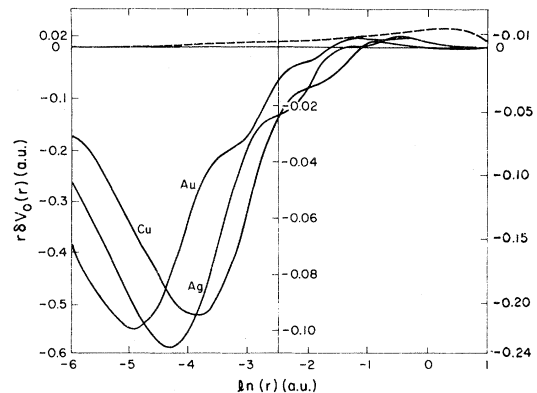
FIG. 5. Changes in the self-consistent crystal poten-
tials due to changes in the xc potential. The solid
curves give the changes due to the relativistic exchange
correction and the dashed curve the change due to the
correlation contribution to the xc potential in Au. The
vertical scales at the left, center, and right of the figure
are for Au, Cu, and Ag, respectively.

tude in the high-density region near the nucleus thereby causing the shift in charge away from the nucleus shown in Fig. 3. For Au we have also shown the attractive contribution to the self-consistent crystal potential due to the local correlation potential. We see that in the outer region of the muffin-tin-sphere the correlation contribution to the crystal potential is larger in magnitude, but nearer the nucleus the rx correction becomes more important. Note that in the outer part of the muffin-tin sphere the rx correction to the self-consistent potential becomes attractive. This feature reflects the reduced screening of the nuclear charge caused by the outward shift of the core electrons in a region where the direct effect of the rx correction is small. The influence of these

changes in the crystal potential on the single-particle eigenvalues is discussed in the next section.

III. SINGLE-PARTICLE EIGENVALUES

A. Core levels

The core-level energies and their dependences on rx corrections and correlation corrections are listed in Table II. For a given orbital the size of the rx correction increases by a factor of ~ 5 in going from Cu to Ag and by a further factor ~ 5 in going from Ag to Au. All rx eigenvalue corrections are positive (i.e., weaker binding) except for those of the 4d and 4f levels of Au; for these levels

TABLE II. Core-level eigenvalues for metallic Cu, Ag, and Au. These eigenvalues were determined by integrating the radial Dirac equation using the spherical part of the crystal potential. Changes in the eigenvalues produced by the rx correction, and in the case of Au the correlation correction as well, are listed. The numbers in parentheses are the rx corrections calculated using the Breit interaction (Ref. 24) in atoms.

(nlj)	Cu		Ag		Au		
	$-\epsilon_{nx}$	$\epsilon_{rx} - \epsilon_{nx}$	$-\epsilon_{nx}$	$\epsilon_{rx} - \epsilon_{nx}$	$-\epsilon_{nx}$	$\epsilon_{rx} - \epsilon_{nx}$	$\epsilon_{xo} - \epsilon_{nx}$
$(1s\frac{1}{2})$	648.3	1.93 (0.86)	1858	8.4 (4.2)	5923	40.1 (23.1)	0.2
$(2s\frac{1}{2})$	77.19	0.17 (0.06)	273.0	0.9 (0.4)	1044	5.7 (2.6)	0.1
$(2p\frac{1}{2})$	67.62	0.09 (0.10)	253.8	0.6 (0.7)	1001	4.9 (4.5)	0.1
$(2p\frac{3}{2})$	66.11	0.08 (0.08)	241.0	0.6 (0.5)	866.1	3.14 (3.0)	0.10
$(3s\frac{1}{2})$	7.632	0.023	49.51	0.15	245.7	1.15	0.07
$(3p\frac{1}{2})$	4.662	0.010	41.87	0.08	226.4	0.89	0.07
$(3p\frac{3}{2})$	4.470	0.009	39.60	0.07	196.7	0.55	0.07
$(3d\frac{3}{2})$			26.01	0.009	164.7	0.22	0.07
$(3d\frac{5}{2})$			25.56	0.008	158.3	0.18	0.07
$(4s\frac{1}{2})$			6.328	0.025	52.66	0.22	0.06
$(4p\frac{1}{2})$			3.909	0.011	44.47	0.14	0.06
$(4p\frac{3}{2})$			3.526	0.008	37.32	0.06	0.06
$(4d\frac{3}{2})$					23.91	-0.02	0.05
$(4d\frac{5}{2})$					22.58	-0.03	0.05
$(4f\frac{5}{2})$					5.358	-0.08	0.05
$(4f\frac{7}{2})$					5.077	-0.08	0.05
$(5s\frac{1}{2})$					7.205	0.012	0.037
$(5p\frac{1}{2})$					4.5371	-0.006	0.035
$(5p\frac{3}{2})$					3.3078	-0.017	0.033

much of the weight of the radial wave function is centered near the attractive region of the rx potential shift noted in Sec. II. Similar results for core-level energy shifts due to rx corrections have recently been reported by Das et al.[23] who have performed self-consistent atomic calculations for neutral uranium and ions of the lithium isoelectronic sequence. (Their rx energy shifts in U are a factor of ~ 2 larger than those obtained here for Au.)

Energy shifts obtained from the rx potential contain field-theoretic contributions which, in the case of atomic calculations, are normally included by using the Breit interaction.[13] More precisely, the rx correction in our work represents a local density approximation to magnetic interactions, retardation corrections to the Coulomb interaction, and corrections to the Dirac-Fock exchange potential. Since, to leading relativistic order, only the magnetic interactions contribute to the rx correction[22] it is natural to compare the rx energy shifts with magnetic interaction contributions to atomic binding energies calculated using the Breit interaction.[24] From Table II the agreement is seen to be very satisfactory except for the s levels where the rx energy shifts are seen to be about a factor of 2 larger. Part of the discrepancy might be thought to result from our use of a point-nucleus approximation in our solid-state calculations.[25] We have checked this by performing atomic calculations using both the point approximation and finite nucleus capability. We find that only the $1s_{1/2}$ results are affected at all appreciably in the LDA. A consistent overestimate of the s-state rx correction does persist which may reflect the failing of the local density approximation in the region near the nucleus. Because of the great simplicity of the local density approximation method of including these field-theoretic corrections, we believe the possibility of improving of the approximation, in the s-state case, should be investigated.

B. Valence levels

We first discuss some qualitative features of our results for the valence-band energy levels and then turn our attention to the small changes produced by the relativistic exchange corrections. The valence-band densities of states are illustrated in Figs. 6—8. The most important feature of these results concerns the width of the d-bands and their position relative to the Fermi level. Our results in this respect have been summarized and compared
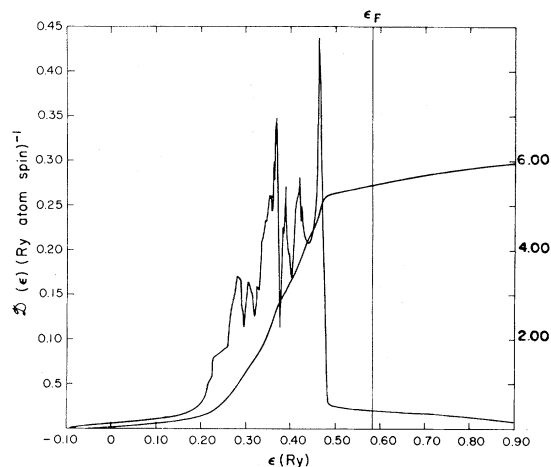
FIG. 6. The valence-band density of states $D(\epsilon)$ and the number of occupied states $N(\epsilon)$ for Cu. The left scale is for $D(\epsilon)$ and the right scale is for $N(\epsilon)$. The spin-orbit correction has been included.

with selected experimental and theoretical work in Table IV. For Cu we have compared with the first-principles calculation of Moruzzi et al.[26] This calculation is similar to ours in that the single-particle equations were solved self-consistently and a local density approximation (LDA) exchange potential was used, but differs in that non-muffin-tin and relativistic effects were excluded. Not surprisingly the d-band widths and positions do not differ greatly. Comparing these results with the experimental values assigned by Knapp et al.[27] on the basis of angular-resolved photoemission (ARP) data suggests that self-consistent treatments with a LDA exchange potential yield d
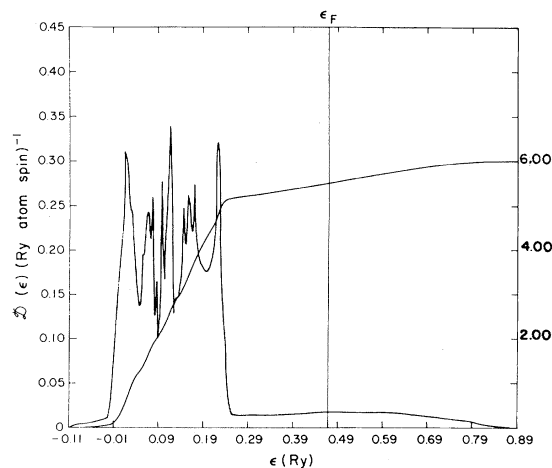
FIG. 7. As in Fig. 6 but for Ag.
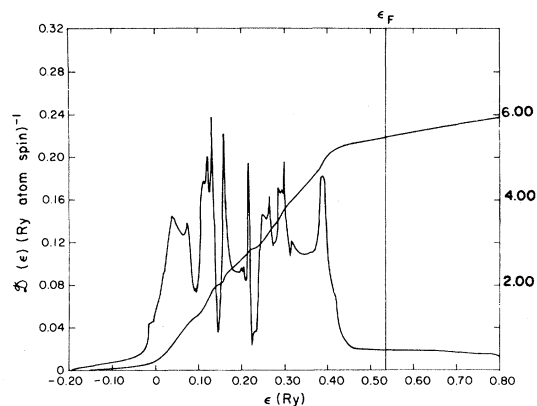
FIG. 8. As in Fig. 7 but for Au.

bands which are both too wide and too weakly bound. This is the same situation which was found to prevail for Pd and Pt.[13] On the other hand, it has been found that the valence-level eigenvalues obtained from non-self-consistent band calculations with crystal potentials constructed from overlapping atomic charge densities (OCD) and a $\alpha = 1$, $X\alpha$ exchange potential agree well with photoemission-assigned values. As an example we have listed the eigenvalues so obtained by Christen-

sen *et al.* for Ag (Ref. 28) and Au (Ref. 29) in Table III. For both Ag and Au the OCD $\alpha = 1$ calculation yields d-band position and widths much closer to those assigned from the photoemission data than the present calculation does. This may be either due to the OCD $\alpha = 1$ eigenvalues being closer to the metal eigenvalues or due to relaxation effects being mimicked by this particular prescription for a non-self-consistent calculation.[13]

For Ag and Cu spin-orbit induced valence-level eigenvalue shifts are $\lesssim 1$ mRy except in those cases where a degeneracy is lifted by the spin-orbit interaction. The larger shifts in Au reflect the fact that in this latter case there is a significant separation of the $j = \frac{3}{2}$ and $j = \frac{5}{2}$ components of the d band.[32] The spin-orbit splittings are compared with experiment in Table IV in terms of an effective crystal-field spin-orbit splitting parameter for the d band ξ_d. The spin-orbit interaction is expected to be stronger near the top of the d band since these wave functions are more localized in the core region.[33] This expectation is fulfilled in our results by the larger value of ξ_d inferred from the splitting of the X_5 level at the top of the d-band compared to that inferred from the splitting

TABLE III. d-band widths and positions in the noble metals. Results have been listed in each case for the three high-symmetry $\vec{k}$ points Γ, L, and X. The width is here defined as the energy difference between the highest and lowest d-band eigenvalues at the $\vec{k}$ point and the position as the highest d-band eigenvalue. All energies are in mRy and are measured with respect to the Fermi energy. Results of this paper have been obtained with the rx potential and for Ag and Au include spin-orbit coupling. OCD refers to calculations with potentials constructed from overlapping atomic charge densities.

	Metal	Γ Position	Width	X Position	Width	L Position	Width
This paper	Cu	−172	60	−116	253	−129	252
MWJ[a]	Cu	−177	59	−119	268	−131	259
Experiment[b]	Cu	−210	59	−151	232	−165	202
This paper	Ag	−295	90	−209	273	−232	250
C-OCD[c]	Ag	−349	85	−274	250	−292	218
Experiment[d]	Ag	−351	84			−291	219
This paper	Au	−233	175	−86	464	−130	435
CS-OCD[e]	Au	−257	170	−121	431	−161	386
Experiment[f]	Au	−261	173				

[a]Reference 26.
[b]Reference 27.
[c]Reference 28.
[d]Reference 30.
[e]Reference 29.
[f]Reference 31.

TABLE IV. Crystal field spin-orbit splitting parameters ξ_d for the noble metals. From the theoretical calculations parameters have been deduced from the splitting of the $\Gamma_{25'}$ level in the middle of the d band and from the splitting of the X_5 level at the top of the d band. These values have been compared with those deduced from photoemission data. All energies are in mRy.

Source	Cu	Ag	Au
Splitting of $\Gamma_{25'}$	9	19	58
Splitting of X_5	11	24	72
ARP (of Γ'_{25})		18 ± 1[a]	52 ± 4[b]

[a]Reference 29.
[b]Reference 30.

of the $\Gamma_{25'}$ level near the bottom of the d band. The agreement between $\Gamma_{25'}$ splitting and the average ξ_d assigned from ARP data is excellent.

For the valence levels the rx contribution leads to a lowering of the d band relative to the s band by about 1.7, 2.9, and 4.8 mRy in Cu, Ag, and Au, respectively. To put these numbers in perspective we note that the correlation contribution to the crystal potential lowers the Au d band by about 15 mRy relative to the s band and that the discrepancies in the d-band positions discussed above are about 30, 55, and 35 mRy for Cu, Ag, and Au, respectively. Thus, for these metals the magnitudes of the rx corrections are appreciable but not sufficiently large to cause any gross change from results obtained with the nx potential. Changes in valence-level properties due to rx corrections are expected to be largest when orbitals of greatly different spatial dependence have similar energies, e.g., in the case of the rare-earth metals.

IV. FERMI SURFACES

The intersections of the Fermi surfaces obtained here with the high-symmetry planes are illustrated in Figs. 9—11. Several calipers of these Fermi surfaces have been used to compare our Fermi surfaces with the accurately known experimental Fermi surfaces in Table V. To the number of figures given, the Fourier fits of Coleridge and Templeton[34,35] are identical to the phase-shift fits of Shaw et al.[36] We first consider the neck radius. This feature of the Fermi surface has been examined in some detail by Janak et al.[37,38] in the case of Cu, who have pointed out that the neck radius given by a nonrelativistic non-muffin-tin calculation with the nx potential is about 10% too large. These authors found that, in using $X\alpha$ potentials, increasing α from the value $\alpha = 0.70$, which corresponds closely with the nx potential in the case of Cu, to the value $\alpha = 0.77$ brings the neck radius into close agreement with experiment. To understand why this occurs we note that a simple effective-

FIG. 9. Fermi-surface intersections with high-symmetry planes in Cu.
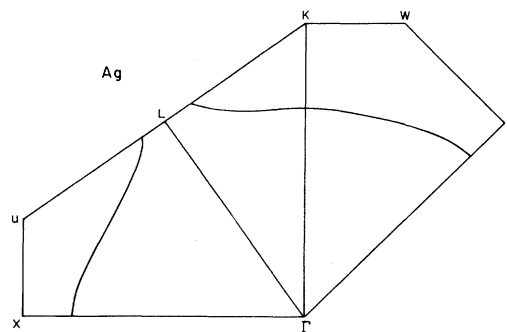
FIG. 10. Fermi-surface intersections with high-symmetry planes in Ag.
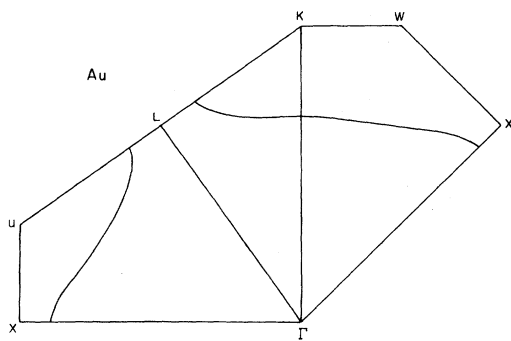
FIG. 11. Fermi-surface intersections with high-symmetry planes in Au.

mass treatment yields $k_N \simeq m^* \, (E_f - E_{L_2'})^{1/2}$ where E_f is the Fermi energy and $E_{L_2'}$ is the energy of the occupied sixth-band state at L. A decrease in neck radius with α implies that E_F decreases with α more quickly than $E_{L_2'}$. Since the increased attractiveness in the potential caused by increasing α is larger in the high-density core region this implies that the d character of L_2' wave function has less weight than for the average Fermi-surface wave function.[39] This observation is consistent with the partial densities of states obtained from Fermi-surface phase-shift fits by Coleridge et al.[40] who point out that the d fraction is very anisotropic over the bellylike portions of Fermi surface (see

below). Comparing the xo and nx potential Fermi surfaces in Au we see that including correlation, which corresponds to increasing α, decreases the neck radius in Au as well. The agreement obtained between nx and experimental neck radii for Au is remarkably good.

The d fraction of the wave function has considerable anisotropy even over the belly portion of the Fermi surface, reaching a maximum in the $\langle 110 \rangle$ direction and a minimum in the $\langle 100 \rangle$ direction. Thus we expect the inclusion of correlation (i.e., going from xo to nx potentials), or equivalently the increase of α in an $X\alpha$ calculation, to increase the Fermi radius in $\langle 110 \rangle$ direction. This is exactly what we observe for the case of Au. See Table V. Parenthetically, note that the spin-orbit interaction also has a sizable impact on the Fermi surface of Au. On the other hand, for Cu we find that the present inclusion of relativistic and non-muffin-tin effects reduces the neck radius discrepancy from about 10% to less than 4%. This is a very pleasing result since the ad hoc increase in α used by Janak et al. would have a detrimental impact on the bulk property results.[41-43] We should note that Jepsen et al.[44] have recently found an 11% discrepancy in the neck radius of Cu in a self-consistent muffin-tin relativistic calculation. In order to compare with this result we have recalculated the Cu neck radius with the non-muffin-tin terms in our crystal potential self-consistently set to zero. When this was done the neck radius

TABLE V. Some Fermi-surface calipers for the noble metals. k_F^{100} and k_F^{110} are the Fermi radii in the $\langle 100 \rangle$ and $\langle 110 \rangle$ directions while k_F^0 is the free-electron Fermi radius. k_F^N is the neck radius on the $\langle 111 \rangle$ face. The theoretical results obtained using nx, rx, and xo potentials are listed. For the nx potential the Fermi surface obtained when the spin-orbit interaction is neglected ($-S0$) is also listed.

		Expt.[a]	nx($-S0$)rx	xo
k_F^{100}/k_F^0	Cu	1.058	1.079(1.078)1.078	
	Ag	1.048	1.059(1.057)1.057	
	Au	1.123	1.146(1.136)1.142	1.156
k_F^{110}/k_F^0	Cu	0.951	0.949(0.949)0.950	
	Ag	0.963	0.968(0.969)0.969	
	Au	0.942	0.948(0.950)0.950	0.944
k_{rad}^N/k_F^0	Cu	0.189	0.193(0.192)0.193	
	Ag	0.136	0.134(0.130)0.133	
	Au	0.179	0.178 0.174	0.186

[a]References 34 and 35.

discrepancy increased to ~7%. The origin of the difference between this result and that of Jepsen *et al.* is uncertain, although it appears that the main difference between the two calculations is that they have used a more approximate procedure in constructing the self-consistent crystal potential. As Jepsen *et al.* have emphasized the neck radius is extremely sensitive to the crystal potential. (In terms of energies the difference corresponds to ~5 mRy for the sixth-band energy at L.) This conclusion has a bearing on attempts to explain this discrepancy on the basis of improved approximation for the self-energy operator of the metal.[45]

The changes in the Fermi surface produced by the relativistic exchange corrections tend to be in the same direction as those produced by the correlation contributions and, in the case of Au, about half as large. The shifts in this case come about because the free electronlike wave functions *are* large enough near the nucleus for the rx correction to raise their energy (where the correlation potential pulls the d states down relative to the plane-wave-like states). These rx corrections move the nx potential Fermi surface slightly toward the experimental Fermi surface in the case of Cu and slightly away from the experimental Fermi surfaces in Ag and Au.

The Fermi-level densities of states obtained here are listed and compared with the experimental specific heats[46] and accepted values for the noble-metal electron-phonon mass enhancement parameters[47] in Table VI. In each case the calculated specific heat masses are larger than those derived

from experimental data. We have made no attempt to include possible modifications in the electron mass due to electron-electron interactions. In the case of Cu, Liu *et al.*[48] have considered these modifications using formulas suggested by Sham and Kohn[2] and Kohn and Sham,[49] both of which involve using the electron-electron modification factor of the electron gas at some average density of the metal. Using recent electron-gas calculations[3] in these formulas would produce small reductions in the specific heat masses for each of the noble metals and result in somewhat better agreement with experiment. In addition, recent work[4] using a more accurate approximation for a simple metal self-energy operator suggests that large mass renormalizations may be produced even when the mass renormalizations in the electron gas of the same density are small. Thus we believe that the discrepancies between theory and experiment in Table VI are of the expected sign for electron-electron renormalizations and have a magnitude which is plausible for an electron-electron renormalization effect.

V. SPIN SUSCEPTIBILITY

The spatial dependence of the spin magnetization densities induced in the noble metals by constant magnetic fields is illustrated in Fig. 12. This figure presents the $L=0$ coefficient in the Kubic harmonic expansion of the induced spin magnetization density $\gamma(\vec{r})$, normalized so that the integral

TABLE VI. The densities of states at the Fermi level $D(\epsilon_F)$ in the noble metals. Results have been listed for both nx and rx potential and, in the case of Au, also the xo potential. The specific-heat effective masses corresponding to these values for $D(\epsilon_F)$ are listed under the column headed by m^*_{theor}. Also listed is the average square velocity over the Fermi surface $V^2(\epsilon_F)$, and the corresponding effective mass m^*_V. m^*_{theor} and m^*_V represent different averages of the electron mass over the Fermi surfaces.

		ϵ_F (mRy)	$D(\epsilon_F)$ ($d\,\text{Ry}^{-1}\text{atom}^{-1}$)	m^*_{theor}	$\langle V^2(\epsilon_F)\rangle$ (a.u.)	m^*_V	m^{*a}_{expt}
Cu	nx	594	3.967	1.375	1.12	1.36	1.21
	rx	595	3.958	1.372			
Ag	nx	462	3.578	0.972	1.84	0.94	0.91
	rx	463	3.575	0.971			
Au	nx	543	3.899	1.062	1.63	1.01	0.91
	rx	546	3.860	1.052			
	xo	563	4.001	1.090			

[a]References 46 and 47.
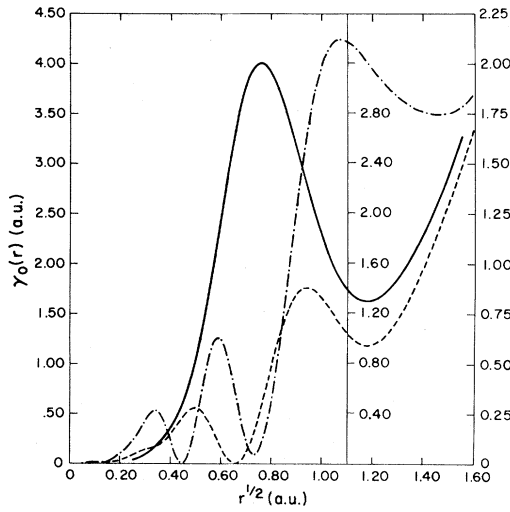
FIG. 12. $\gamma_0(r)$ for Cu, Ag, and Au. $\gamma_0(r)$ is the angular average of the induced magnetization inside the muffin-tin sphere. The solid curve is for Cu, the dashed curve for Ag, and the chained curve for Au. The vertical scales at the left, center, and right of the figure refer to Cu, Ag, and Au, respectively.

of $\gamma(\vec{r})$ over one unit cell is 1. $\gamma(\vec{r})$ is proportional to the contribution to the charge density from electrons at the Fermi surface. From Fig. 12 we see that the atomiclike d-band contribution to $\gamma(\vec{r})$ is larger in Cu and Au than in Ag. The more free-electronlike character in Ag is expected since, as pointed out earlier, the d bands are farther below the Fermi surface.

These induced magnetization distributions enter when calculating the spin susceptibility from the variationally based expression of Vosko and Perdew.[50] Our results for the spin susceptibility are listed in Table VII, and compared with values deduced from the Landau level spin-splitting measurements of Bibby and Schoenberg.[51,52] The agreement is excellent except for Au. In that case the large spin-orbit coupling partially invalidates our treatment of the spin susceptibility as evidenced by the large variations in the g factor observed experimentally.[53] It should be emphasized that for all three metals the exchange-correlation enhancement is much weaker than that for the corresponding electron-density uniform gas. Thus we believe the frequently adopted approach of estimating many-body influences in the noble metals by referring directly to the corresponding uniform gas (e.g., Ref. 54) is misleading.

VI. SUMMARY AND CONCLUSIONS

For each of the noble metals, we have solved the relativistic Kohn-Sham single-particle equations, self-consistently including non-muffin-tin terms in the crystal potential. Of the quantities we have calculated, the electron-number density and the Pauli magnetic susceptibility depend only on the adequacy of the LDA for the xc energy functional for their reliability. For Cu we were able to compare our calculated scattering form factors with experiment and found close agreement ($<2\%$), although a tendency toward larger form factors (more contracted charge densities) was noted in the theoretical results. The same level of agreement ($\sim 2\%$) was obtained in comparing theoretical and experimental Pauli susceptibilities.

Theoretically the identification of the Fermi surface calculated from the Kohn-Sham eigenvalues

TABLE VII. The Pauli susceptibility in the noble metals. I is the density functional Stoner parameter. S is the exchange-correlation enhancement factor.

Metal	Potential	$D(\epsilon_F)$ $(d\,\mathrm{Ry}^{-1}\mathrm{atom}^{-1})$	I (mRy)	χ_P (emu/mole)	$\chi_P^{\mathrm{expt\,a}}$ (emu/mole)	S 1.096
Cu	nx	3.967	22.1	10.33	10.1	1.096
Cu	rx	3.958	22.1	10.31		
Ag	nx	3.578	18.9	9.12	9.0	1.073
Ag	rx	3.575	18.9	9.11		1.073
Au	nx	3.899	15.3	9.86	10.1	1.063
Au	rx	3.860	15.3	9.75		1.063
Au	xo	4.001	15.3	10.13		1.065

[a]Reference 46.

with the experimental Fermi surface requires approximations in addition to the LDA.[2] Our results indicate that the agreement between experiment and our first-principles Fermi surfaces in the noble metals is remarkably good (see Table V). In the worst case, Cu, the discrepancy between theory and experiment is only $\sim 2\%$ for typical Fermi-surface calipers. Even the neck radius, a more sensitive Fermi-surface index, was found to be given more accurately than what would have been expected on the basis of nonrelativistic non-muffin-tin calculations. In fact, the deviations of the noble-metal Fermi surfaces from sphericity are much more accurately rendered by single-particle theory than the corresponding deviations for the alkali metals.[4]

On the other hand, for energies away from the Fermi surface and the associated excitation energies of the solid, discrepancies between the single-particle interpretation of Kohn-Sham eigenvalues and experiment are evident. The d bands inferred from our valence-level eigenvalues are too weakly bound and too broad compared to experiment. The same relationships held in our earlier work in Pd and Pt.[13] As we have noted, closer agreement with photoemission-assigned d bands is obtained from non-self-consistent OCD $\alpha = 1$ calculations. We believe this situation can be understood in terms of the comparison between the corresponding atomic calculations, in which the use of full Slater exchange was found to simulate relaxation effects in the eignevalue differences.

One objective of this paper was to examine the influence of the relativistic correction to the exchange potential which appears in the relativistic generalization of the density functional formalism[9,10] for the noble metals. This correction is not large enough to induce any qualitative changes in electronic properties but does produce quantitative changes on roughly the same scale as those due to the correlation contribution to the potential. By comparing our rx core eigenvalue shifts with the corresponding atomic eigenvalue shifts calculated using the Breit interaction we were able to demonstrate that the rx correction is given accurately except in the case of s levels; it is our hope that the LDA rx potential can be altered in a way which will remove this difficulty. For the valence-level eigenvalues the rx energy shifts are, at least in the case of Au, comparable to those produced by the correlation potential. Since much effort has been devoted to obtain accurate forms for the correlation potential, we suggest that the equally important rx correction should be included in relativistic electronic structure calculations, especially for systems containing atoms at the upper end of the periodic table.

ACKNOWLEDGMENTS

*Present address: Physics Department, McMaster University, Hamilton, Canada L8S 4M1.

[1]For example, see A. K. Rajagopal in, *Advances in Chemical Physics*, edited by I. Prigogine and S. A. Rice (Wiley, New York, 1974), Vol. 41; W. Kohn and P. Vashista, in *Physics of Solids and Liquids*, edited by S. Lundqvist and N. H. March (in press).

[2]L. J. Sham and W. Kohn, Phys. Rev. 145, 561 (1966).

[3]A. H. MacDonald, M. W. C. Dharma-wardana, and D. J. W. Geldart, J. Phys. F 10, 1719 (1980).

[4]A. H. MacDonald, J. Phys. F 10, 1737 (1980).

[5]M. Rasolt, S. B. Nickerson, and S. H. Vosko, Solid State Commun. 16, 827 (1975).

[6]M. Rasolt and S. H. Vosko, Phys. Rev. B 10, 4195 (1974).

[7]M. Rasolt and S. H. Vosko, Phys. Rev. Lett. 32, 297 (1974).

[8]G. Arbman and U. von Barth, J. Phys. F 5, 1155 (1975).

[9]A. K. Rajagopal, J. Phys. C 11, L943 (1978).

[10]A. H. MacDonald and S. H. Vosko, J. Phys. C 12, 2977 (1979).

[11]This form of parametrization for μ_{xc} was first proposed by L. Hedin and B. I. Lundqvist, J. Phys. C 4, 2064 (1971). The values of A and C used here were A = 11.4 and C = 0.066 after O. Gunnarsson, B. I. Lundqvist, and J. W. Wilkins, Phys. Rev. B 10, 1319 (1974). These parameters give correlation contributions similar to those implied by a number of recent electron-gas calculations (see Ref. 3). A different form of parametrization has recently been suggested by S. H. Vosko, L. Wilk, and M. Nusair, Can. J. Phys. 58, 1200 (1980). This latter form, when fit to the Monte Carlo results of Ceperley and Alder provides the most accurate characterization of correlation energy density dependence currently available.

[12]In a previous article (Ref. 13) the expression for a related relativistic correction factor was inadvertently

listed as the expression for ψ^{rx}. The correct expression was used in all calculations.

[13]A. H. MacDonald, J. M. Daams, S. H. Vosko, and D. D. Koelling, Phys. Rev. B 23, 6377 (1981).

[14]A. H. MacDonald, S. H. Vosko, and P. T. Coleridge, J. Phys. F 12, 2991 (1979).

[15]See N. Elyashar and D. D. Koelling, Phys. Rev. B 15, 3620 (1977).

[16]J. R. Schneider, N. K. Hansen, and H. Kretschmer Acta. Crystallogr. (in press); see also G. Mazzone, Phys. Rev. B 23, 3840 (1981).

[17]L. D. Jennings, D. R. Chipman, and J. J. De Marco, Phys. Rev. 135, 1612 (1964).

[18]A. Freund, Ph.D. thesis, Technische Universitat München, 1973, as quoted in Ref. 16 (unpublished).

[19]E. C. Snow, Phys. Rev. 171, 785 (1968); 172, 708 (1968).

[20]F. J. Arlinghaus, Phys. Rev. 153, 743 (1967).

[21]R. J. Weiss, Philos. Mag. B38, 645 (1978); S. Wakoh and T. Yamashita, J. Phys. Soc. Jpn. 35, 1394 (1973).

[22]A. H. MacDonald, Ph.D. thesis, University of Toronto, 1978 (unpublished).

[23]M. P. Das, M. V. Ramana, and A. K. Rajagopal, Phys. Rev. A 22, 9 (1980).

[24]For example, K-N Huang, M. Aoyagi, M. H. Chen, B. Crasemann, and H. Mark, At. Data Nucl. Data Tables 18, 243 (1976).

[25]The magnetic-interaction contribution to orbital binding energies is known to be sensitive to approximations made for nuclear charge distributions. See, e.g., F. T. Porter and M. S. Freedman, J. Phys. Chem. Ref. Data 7, 1267 (1978).

[26]V. L. Moruzzi, A. R. Williams, and J. F. Janak, Calculated Electronic Properties of Metals (Pergamon, New York, 1978).

[27]J. A. Knapp, F. J. Himpsel, and D. E. Eastman, Phys. Rev. B 19, 4952 (1979).

[28]N. E. Christensen, Phys. Status. Solidi B 54, 551 (1972).

[29]N. E. Christensen and B. O. Seraphin, Phys. Rev. B 4, 3321 (1971); N. E. Christensen, ibid. 13, 2698 (1976).

[30]P. S. Wehner, R. S. Williams, S. D. Kevan, D. Denley, and D. A. Shirley, Phys. Rev. B 19, 6164 (1980).

[31]K. A. Mills, R. F. Davis, S. D. Kevan, G. Thornton, and D. A. Shirley, Phys. Rev. B 22, 581 (1980).

[32]N. E. Christensen, J. Phys. F 8, L51 (1978).

[33]A. H. MacDonald, W. E. Pickett, and D. D. Koelling, J. Phys. C 13, 2675 (1980).

[34]P. T. Coleridge (private communication).

[35]P. T. Coleridge and I. M. Templeton, J. Phys. F 2, 643 (1972).

[36]J. C. Shaw, J. B. Ketterson, and L. R. Windmiller, Phys. Rev. B 5, 3894 (1972).

[37]J. F. Janak, A. R. Williams, and V. L. Moruzzi, Phys. Rev. B 6, 4367 (1972).

[38]J. F. Janak, A. R. Williams, and V. L. Moruzzi, Phys. Rev. B 11, 1522 (1975).

[39]Symmetry considerations imply that there is no s character in the L_2' wave function. Thus the more free-electron part of the wave function has p character.

[40]P. T. Coleridge, N. A. W. Holzwarth, and M. J. G. Lee, Phys. Rev. B 10, 1213 (1974); P. T. Coleridge (private communication).

[41]E. C. Snow, Solid State Commun. 13, 1775 (1973).

[42]E. C. Snow, Phys. Rev. B. 8, 5391 (1973).

[43]J. Janak, V. L. Moruzzi, and A. R. Williams, Phys. Rev. B 12, 1257 (1975).

[44]O. Jepsen, D. Glotzel, and A. R. Mackintosh, Phys. Rev. B 23, 2684 (1981).

[45]S. Y. Wang and M. Rasolt, Phys. Rev. B. 15, 3714 (177).

[46]D. L. Martin, Phys. Rev. B 8, 5357 (1973).

[47]G. Grimvall, Phys. Scr. 14, 63 (1976).

[48]K. L. Liu, A. H. MacDonald, and S. H. Vosko, Can. J. Phys. 55, 1991 (1977).

[49]W. Khon and L. J. Sham, Phys. Rev. 140, A1133 (1965).

[50]S. H. Vosko and J. P. Perdew, Can. J. Phys. 53, 1385 (1975).

[51]W. M. Bibby and D. Shoenberg, J. Low Temp. Phys. 34, 659 (1979).

[52]W. M. Bibby and D. Shoenberg, Phys. Lett. 60A, 235 (1977).

[53]G. W. Crabtree, L. R. Windmiller, and J. B. Ketterson, J. Low Temp. Phys. 20, 655 (1975).

[54]R. Singh, S. Prakash, and J. Singh, J. Phys. F 10, 1249 (1980).